Nanoaperture-enhanced fluorescence: Towards higher detection rates with plasmonic metals

Davy Gérard, Jérôme Wenger, Nicolas Bonod, Evgeni Popov, and Hervé Rigneault
Institut Fresnel, CNRS UMR 6133, Domaine Universitaire de Saint-Jérôme, 13397 Marseille Cedex 20, France

Farhad Mahdavi and Steve Blair
Electrical and Computer Engineering Department, University of Utah, 50 S. Central Campus Drive, Room 3280, Salt Lake City, Utah 84112, USA

José Dintinger and Thomas W. Ebbesen
Institut de Science et d'Ingénierie Supramoléculaire, CNRS UMR 7006, Université Louis Pasteur, 8 allée G. Monge, 67000 Strasbourg, France

(Received 6 November 2007; published 17 January 2008)

A bare nanometric aperture milled in a metallic film forms a simple nanophotonic device that can strongly enhance the optical properties of nearby emitters such as fluorescent molecules. In this paper, we experimentally and numerically compare the properties of circular apertures milled in gold and aluminum, and discuss the influence of a noble metal holding plasmonic resonances in the visible range such as gold. We report that nanometric apertures milled in gold exhibit significantly higher fluorescence enhancement factors than apertures in aluminum. We relate this effect to a larger enhancement of the excitation intensity and radiative rate for an aperture milled in gold. A spectrally resolved analysis of the fluorescence emission from apertures is also presented. Comparison with numerical simulations shows that the enhancement factor is maximum when the photonic density of modes is maximum. Altogether, these results provide crucial knowledge for the design of nanoapertures towards high-efficiency single-molecule analysis.

DOI: 10.1103/PhysRevB.77.045413 PACS number(s): 78.67.−n, 33.50.−j, 82.37.−j, 42.50.−p

I. INTRODUCTION

A bare subwavelength aperture milled in a metallic film forms a simple nanophotonic device. However, in spite of its conceptual simplicity, it exhibits complex and interesting optical properties. As soon as one is dealing with nanosized apertures pierced in a finite-thickness real metal, Bethe's theory[1] is no longer valid and a rigorous diffraction theory must be employed. A number of intriguing phenomena have been experimentally observed, such as the so-called extraordinary transmission through arrays of holes or slits,[2,3] directivity of the transmission through a single structured aperture,[4] or electromagnetic field enhancement and confinement inside and in the vicinity of the aperture.[5,6] All these phenomena are of practical significance to develop new applications in photonics, nano-optics, and biophotonics. In the years immediately following the first report of extraordinary transmission,[2] most of the attention was attracted by the properties of periodic arrays of holes or slits. More recently, there has been a growing interest around the properties of single (i.e., isolated) nanoapertures.[7] Indeed, a single nanoaperture can exhibit a surprisingly high transmission; it also supports highly confined and enhanced electromagnetic fields. Both properties arise from the existence, even for very small holes, of guided modes inside the aperture.[8–12]

The presence of high amplitude electromagnetic fields inside nanoapertures makes them promising for enhancing the fluorescent emission from molecules or nanocrystals. Many groups have already reported fluorescent emission enhancement from emitters located in the vicinity of different types of metallic nanostructures: metallic nanoparticles,[13–19] nanoporous gold,[20] gold "nanopockets,"[21] hole arrays and metallic gratings,[22–26] and single nanoapertures.[27–29] In this paper, we will focus our attention on subwavelength apertures. Such nanostructures present a certain number of advantages. First, they can be fabricated with robust nanofabrication techniques; consequently, the size and shape of the apertures are controlled and reproducible. Second, rigorous simulation algorithms of the electromagnetic properties of apertures are available. The last advantage is linked to the geometry of the aperture: it acts as a small reaction chamber and is a convenient platform that allows highly parallel solution analysis[30,31]—a crucial issue for biological applications.[32,33]

The fluorescence emission of an emitter located inside a nanoaperture may be affected in two ways: (i) by the local enhancement of the excitation intensity, and (ii) by the modification of the electromagnetic environment of the emitter, changing its quantum efficiency and radiation pattern. In both effects, surface plasmons can play a positive role to yield larger fluorescence rates.[13,34] In previous experiments,[28,29] only apertures milled in aluminum films were studied, yet aluminum does not sustain significant plasmonic effects in the visible range. Can we expect an increase of the enhancement factor in the case of a metal supporting strong surface plasmon resonances in the visible range, such as gold? To address this issue, we report in this paper a detailed comparison between the fluorescence emission enhancement factors for two metals: aluminum and gold. We set the excitation wavelength to 633 nm and use Alexa-Fluor 647 as a fluorescent reporter (Alexa-Fluor 647 is a commonly used dye with emission spectrum ranging from 650 to 710 nm and peak emission at 670 nm).

In order to get an accurate estimation of the fluorescence enhancement factor, it is of crucial importance to quantify the total fluorescence intensity *and* the number of emitters. Fluorescence correlation spectroscopy (FCS) is a robust

method that answers this issue.[35] FCS provides access to the count rate per molecule, that is, the average number of photons emitted by a *single* fluorescent molecule. In this paper, we use FCS to directly compare the fluorescent enhancement from different nanostructures without making any implicit hypothesis on the number of fluorescent molecules.

The paper is outlined as follows. In Sec. II, we present the materials and methods used throughout the paper. A more detailed presentation of the FCS technique is provided. Experimental results are presented in Sec. III. Section IV is devoted to a discussion of the results and to a comparison with electromagnetic calculations. The respective roles of the reinforcement of the excitation intensity and of the modification of the emission characteristics are also discussed. Finally, in Sec. V, we summarize our conclusions.

II. MATERIALS AND METHODS

Optically thick metallic films (thickness of 200 nm) of gold and aluminum were coated on conventional microscope coverslips (thickness of 150 μm) by thermal evaporation. A 15 nm thick chromium layer ensures adhesion between the gold film and the borosilicate glass substrate. No chromium adhesion layer was used for the aluminum samples. Circular apertures with diameters ranging from 80 to 310 nm were then milled by focused ion beam (FEI Strata DB235, using Ga^+ ions exhibiting a 5 nm nominal beam diameter). A sample aperture milled in a gold film is displayed in the inset of Fig. 1(a).

As discussed above, for a rigorous characterization of the fluorescence enhancement, it is necessary to estimate the number of emitting molecules, motivating the use of the FCS technique. The temporal fluctuations $F(t)$ of the fluorescence signal are recorded, and the autocorrelation of this signal is computed:

$$g^{(2)}(\tau) = \frac{\langle F(t) \cdot F(t+\tau) \rangle}{\langle F(t) \rangle^2}, \tag{1}$$

where $\langle \cdot \rangle$ stands for time averaging. A sample correlogram $g^{(2)}(\tau)$ recorded in a nanoaperture is given in Fig. 1(b). The analysis of the experimental data relies on a numerical fit based on a three-dimensional Brownian diffusion model:

$$g^{(2)}(\tau) = 1 + \frac{1}{N}\left(1 - \frac{\langle B \rangle}{\langle F \rangle}\right)^2 \left[1 + n_T \exp\left(-\frac{\tau}{\tau_{b_T}}\right)\right] \times \frac{1}{(1+\tau/\tau_d)\sqrt{1+s^2\tau/\tau_d}}, \tag{2}$$

where N is the total number of molecules, $\langle F \rangle$ the total signal, $\langle B \rangle$ the background noise, n_T the amplitude of the dark state population, τ_{b_T} the dark state blinking time, τ_d the mean diffusion time, and s the ratio of transversal to axial dimensions of the analysis volume. Note that, strictly speaking, the assumption of a free three-dimensional diffusion model is not fulfilled within an aperture. However, this discrepancy can be taken into account by setting the aspect ratio s as a free parameter: it converges to a value close to unity for each run. It is clear from Fig. 1(b) that this model fits remarkably well the experimental data. From the correlogram and Eq. (2), it is possible to compute the count rate per molecule (i.e., the average number of photons emitted by a single molecule) as $\mathrm{CR} = (\langle F \rangle - \langle B \rangle)/N$. Then, the fluorescence enhancement η is given by the ratio of the count rate per molecule measured in the case of an aperture and in the case of an open solution. We point out that all the presented fluorescence data are spatially averaged over all the possible molecule orientations and positions inside the detection volume.

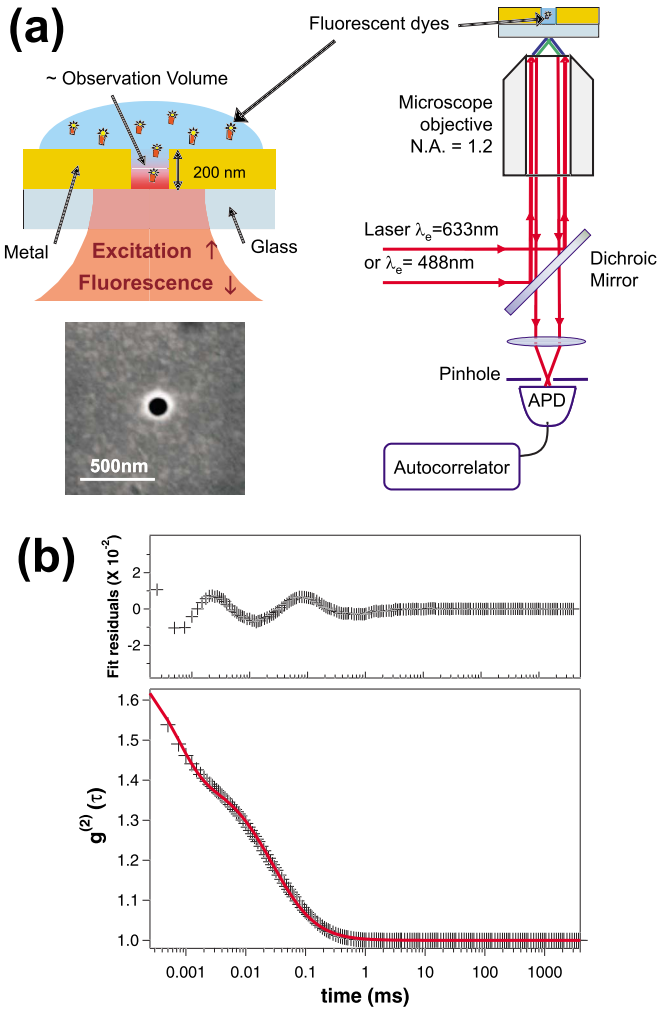

FIG. 1. (Color online) (a) Schematics of the experimental setup (APD, avalanche photodiode). Inset: Micrograph of a single nanoaperture milled in a gold film. (b) Sample correlogram recorded on a nanoaperture: autocorrelation function of the fluorescence emission signal recorded from A647 dyes in a 120 nm circular gold aperture. On the upper part of the graph are plotted the fit residuals.

Our experimental setup has already been presented in Ref. 28, but it is recalled in Fig. 1(a) for completeness. It is based on an inverted microscope (Zeiss Axiovert 35M) with a NA=1.2 water-immersion objective (Zeiss C-Apochromat). For experiments in solution, a 50 μm pinhole defines a three-dimensional detection volume. Nanopositioning of the aperture inside this confocal volume is performed with a multiaxis piezoelectric stage (Polytek PI P527). After the pinhole, the fluorescence signal passes through a 50/50

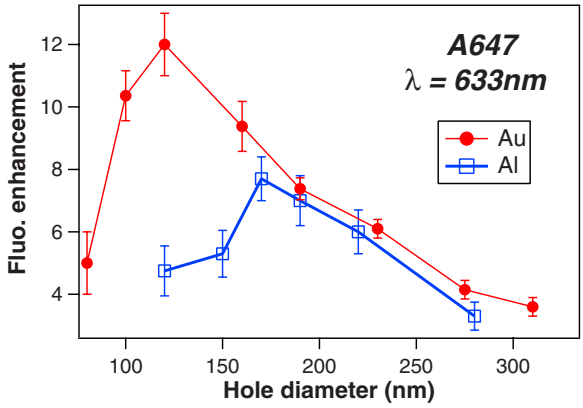

FIG. 2. (Color online) Enhancement factor as a function of the aperture diameter for Alexa-Fluor 647 dyes at λ_e=633 nm (excitation power of 40 μW) for nanoapertures milled in aluminum (squares) and gold (circles) films.

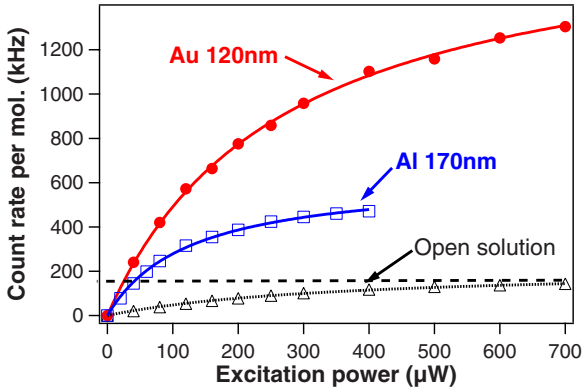

FIG. 3. (Color online) Count rate per molecule as a function of the excitation power at λ_e=633 nm, for A647 dyes diffusing in a 120 nm diameter aperture in a gold film (circles), in a 170 nm diameter aperture in aluminum (squares), or in open solution (triangles). Solid lines are numerical fits by a three-level system (see text). Fitting parameters are for open solution, A=0.6 kHz/μW and I_s=390 μW; for aluminum, A=5.0 kHz/μW and I_s=130 μW; and for gold, A=6.8 kHz/μW and I_s=260 μW.

beamsplitter and is focused on two avalanche photodiodes (Perkin-Elmer SPCM-AQR-13) with 670±20 nm fluorescence bandpass filters (Omega Filters 670DF40). The fluorescence intensity fluctuations are analyzed by cross correlating the signal of each photodiode with an ALV6000 hardware correlator. This configuration eliminates correlations due to the dead time of the photodiodes (50 ns) and avoids artifacts. Each individual FCS measurement was obtained by averaging ten runs of 10 s duration.

For experiments in apertures, a droplet of solution containing Alexa-Fluor 647 fluorescent molecules (A647) is deposited onto the top of the aperture, with typically micromolar concentration. Note that the droplet acts as a reservoir of "fresh" molecules, which are constantly diffusing from the droplet to the aperture. This strongly limits photobleaching effects. Let us also emphasize that in all the following experiments, the signal-to-noise ratio was kept at values better than 10.

III. EXPERIMENTAL RESULTS

A. Fluorescence rate enhancement

We have measured the fluorescence count rate enhancement factor η as a function of the diameter of the aperture for two sets of apertures: the first set milled in an aluminum film, and the other set milled in gold (Fig. 2). The excitation wavelength is set to λ_e=633 nm. We stress that all the values of η presented in Fig. 2 have been measured at low excitation intensity (40 μW) to ensure that the dyes are well below saturation. Both curves have a similar shape: starting from relatively low (~4) enhancement factors for small apertures, the curves quickly rise to a maximum and then decrease for larger aperture diameters. However, regardless of the aperture size, gold always gives a higher enhancement than aluminum. Most interestingly, it reaches a maximum value that is 55% higher than the value observed for aluminum ($\eta_{max}\sim 12$ for gold and $\eta_{max}\sim 7.7$ for aluminum). It should also be noted that the optimal diameter is shifted towards significantly smaller hole sizes for gold (120 nm) compared to aluminum (170 nm). The physics behind this behavior will be discussed in Sec. IV. It can, however, already be concluded that working with apertures milled in gold rather than aluminum brings two advantages. First, the fluorescence emission enhancement factor is significantly higher. Second, it allows us to work at smaller diameters and, consequently, at higher concentrations while keeping single molecule resolution.

Nanoapertures allow for high count rates per molecule, even at moderate incoming excitation powers. We have performed a set of measurements of the count rate per molecule while increasing the excitation power. Please note that special care has been taken to characterize the level of background noise and the dark state fraction n_T for each excitation power. Results are presented in Fig. 3, in the case of an open solution and in the case of apertures milled in gold or aluminum. For aluminum, we limited the excitation power to 400 μW to avoid damaging the sample, as aluminum has a damage threshold about ten times lower than gold. Without the nanostructure, the count rates are limited to values below 180 000 counts per second (cps) per molecule (horizontal line in Fig. 3). In contrast, a striking count rate better than 1 200 000 cps/molecule is obtained in the nanoaperture milled in gold at high excitation power. For aluminum, the maximum rate reaches about 400 000 cps/molecule. Therefore, at fluorescence saturation, a three times higher count rate per molecule can be extracted in gold apertures as compared to aluminum.

To model this experimental data, we use the standard expression of the fluorescence rate of a three level system summarized by $F=A\frac{I_e}{1+Ie/I_s}$, where I_e is the excitation intensity, I_s is the saturation intensity, and A is a constant proportional to the dye absorption cross section, its quantum yield, and the setup collection efficiency.[35] Good agreement between this model and the experimental data is found. This analysis brings some insights in the photokinetic rate enhancements

induced by the nanostructure, as we will discuss in Sec. IV. Before we move on to that discussion, we describe further experimental investigations towards alterations of the spectrum and directivity of the detected fluorescence beam.

B. Spectral analysis

When an emitter is placed near an arbitrary object or inside a cavity, its emission spectrum may be altered.[26,39] The data reported in Fig. 2 correspond to a spectral integration from 650 to 690 nm, which covers most of the dye emission spectrum but prevents any indirect observation of an alteration of the emission spectrum. To detail the fluorescence spectrum, we first performed a FCS measurement to quantify the average number of molecules inside the nanoaperture. Then, with a flipping mirror, the fluorescence beam was sent to a spectrograph (Jobin-Yvon SPEX 270M) equipped with a nitrogen-cooled charge coupled device (CCD) detector. The raw spectrum is eventually normalized by the number of molecules given by FCS. This procedure allows us to directly compare the intensities obtained *per single molecule* for different aperture sizes.

Normalized fluorescence spectra per A647 molecule measured in open solution and on several apertures in a gold film are presented in Fig. 4(a). The detected count rate per molecule is significantly enhanced over the whole A647 emission spectrum, with a maximum enhancement for 120 nm diameter apertures, as observed in FCS. Interestingly, the shapes of the spectra do not change noticeably between open solution and the different apertures. The same behavior has been observed for apertures in aluminum (data not shown). In Fig. 4(b), we plot the spectrally dependent enhancement factor (that is, the ratio of the spectrum recorded for an aperture by the reference spectrum in open solution). Within the range of 650–690 nm, the apparent value of η slightly increases with the wavelength, showing a higher enhancement for redshifted wavelengths. Our data also indicate that the optimal emission wavelength yielding the larger enhancement tends to be redshifted while increasing the aperture size, hereby confirming an intuitively expected scaling effect.

As already pointed out for nanoaperture arrays,[26] no direct correlation can be found between the white light transmission through the aperture and the fluorescence spectra. In the case of our study, we point out that white light transmission measurements through a single aperture of diameter 120–300 nm yielded transmission curves almost flat over the 650–710 nm spectral range covered by the dye emission. This range, therefore, seems too narrow to monitor any clear spectral link between white light transmission and fluorescence.

C. Fluorescence radiation pattern

A nanoaperture may strongly modify the radiation pattern of emitters placed inside it. For instance, Lezec *et al.*[4] have reported an unusual "beaming" effect in the transmitted light from nanoapertures decorated with a periodic set of grooves. In our case, a beaming effect—by concentrating light in a reduced emission cone[36,37]—would increase the molecular

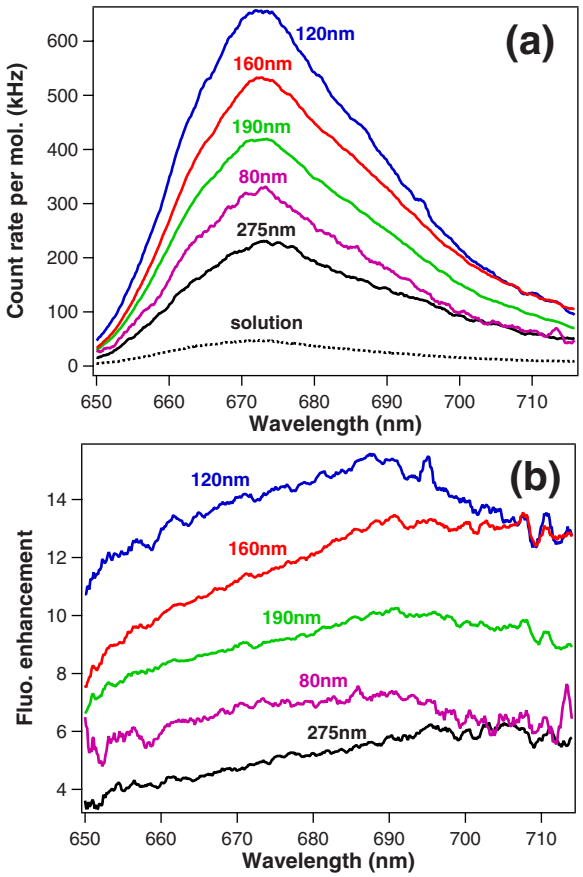

FIG. 4. (Color online) Spectral analysis of the fluorescence enhancement for A647 dyes diffusing in apertures milled in a gold film. (a) Integrated count rate per molecule vs emission wavelength, for a 10 s acquisition time. (b) Fluorescence enhancement factor vs emission wavelength.

detection efficiency and, thus, the enhancement factors exhibited by gold and aluminum. In order to check experimentally the directivity of the fluorescence emission, we have modified our setup to image the microscope objective back focal plane on a CCD camera equipped with fluorescence filters.[38] This configuration allows us to directly monitor the fluorescence radiation pattern from an aperture. It should be emphasized that the numerical aperture of the microscope objective limits the collection to a cone of 64° half-angle. We present in Fig. 5 pictures of the A647 fluorescence beam from a 130 nm diameter hole milled in gold and a 170 nm hole milled in aluminum—these diameters correspond to the maximum enhancement factors. In both cases, the dye's emission fills the back aperture of the microscope objective. Within the collection angle of the microscope, we could not detect any clear effect.

According to recent calculations,[40] the far-field directivity of the beam transmitted through a single subwavelength aperture is highly dependent on the hole size and on the permittivity of the material surrounding the aperture. The directivity of the beam tends to increase when the modulus of the permittivity decreases and when the aperture size increases. In the case of Fig. 5, gold has a lower permittivity than aluminum, but the hole milled in gold is smaller than the one

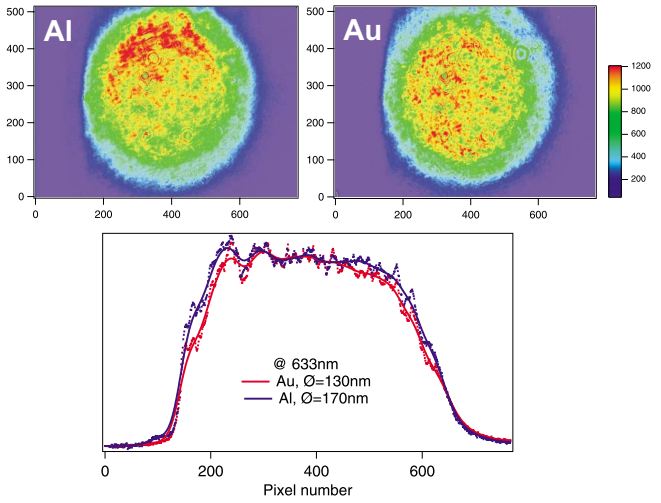

FIG. 5. (Color online) Images of the fluorescence emission beam in the microscope objective back focal plane. Up: CCD pictures of the beam emitted from a 170 nm hole milled in aluminum and a 130 nm hole milled in gold. Bottom: Line cuts of these pictures along a horizontal line (dots, raw experimental data; solid lines, smoothing of the raw data).

milled in the aluminum film. Altogether, the competition between these two effects leads to a similar far-field directivity for both apertures.

IV. DISCUSSION

A natural question while comparing the properties of gold versus aluminum apertures addresses the origin of the higher fluorescence count rates observed for gold. As stated in the Introduction, the fluorescence enhancement observed in Fig. 2 can be induced by a locally increased excitation intensity, by a larger quantum efficiency of the emitter (increased radiative rate vs nonradiative decays), and by a better collection of the emitted light within the objective's numerical aperture. For this last effect, our measurements of the fluorescence radiation pattern indicate that both metals show a similar behavior, with almost identical collection efficiencies. This invalidates any beaming effect linked with gold.

The trends shown by the molecular count rate versus the excitation power yield more insights. At saturation, the fluorescence rate is proportional to the radiative rate and no longer depends on the excitation rate. Therefore, the behavior seen in Fig. 3 for excitation powers above 300 μW shows a net enhancement of the radiative rate for gold apertures versus aluminum. Numerical fitting of the data displayed in Fig. 3 indicates a gain in emission of 7.8 for gold and 2.8 for aluminum. We, thus, conclude that a metal holding plasmonic resonances in the visible range allows for higher emission rates, even if the emission spectra are not significantly modified by the nanostructure.

Things get more intricate at low excitation powers (well below fluorescence saturation), as the fluorescence signal is proportional to the quantum yield of the dye and the excitation power. Previous theoretical analysis on aluminum apertures has shown that excitation enhancement played a critical

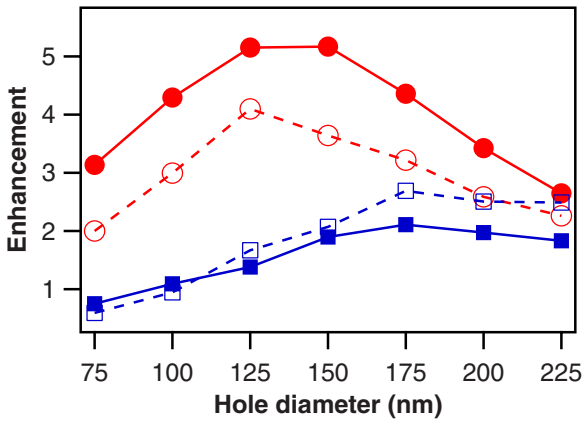

FIG. 6. (Color online) Enhancement factors versus the aperture diameter computed by the finite element method and averaged over a plane 15 nm inside the aperture. Circles refer to gold, squares to aluminum. Empty markers denote excitation gains, filled markers stand for emission.

role in the overall fluorescence gain.[5] From an experimental point of view, it is extremely difficult to estimate the relative weight of the contributions from the excitation and quantum yield. Therefore, we conducted a numerical analysis based on the finite element method using COMSOL MULTIPHYSICS version 3.3.[42] The size of the computational space is $1.0\times1.0\times1.1$ μm^3, with radiation boundary conditions on all six faces. A quartz substrate is assumed, on top of which a 200 nm thick layer of gold or aluminum is placed, the upper region being water. Dielectric properties of gold and aluminum are incorporated via the complex dielectric constant, as measured by spectroscopic ellipsometry from 300 to 1600 nm.[42] A single nanoaperture is placed in the center of the metal layer. To simplify the numerical computations, we restricted the observation area to a plane 15 nm inside the aperture. This provides the trends for the relative contribution of emission and excitation, and avoids normalization issues over the entire aperture volume. Quantitative comparison between experimental data and numerical computations integrated over the entire aperture volume will form the basis of a future communication.

To estimate the increase of the excitation intensity over the nanoaperture, a plane wave at 633 nm is launched 500 nm below the structure, incoming from the glass side. Light intensity is measured and averaged over the plane 15 nm inside the aperture. This result is then normalized by the integrated intensity within the same surface with no metal layer. Results for gold and aluminum films are displayed in Fig. 6 versus the aperture diameter (empty markers). These curves are qualitatively consistent with the experimental data found in Fig. 2, and show a remarkable agreement with the aperture diameters found for maximum fluorescence enhancement. A clear increase of the excitation intensity is found to occur inside the aperture for a diameter below the half-wavelength as already known from Ref. 5. Remarkably, the averaged excitation intensity is about 40% higher for a 120 nm aperture in gold as compared to a 170 nm aperture in aluminum (comparable to 55% observed experimentally). This factor directly contributes to the better

fluorescence enhancement measured for gold apertures at low excitation powers.

For the emission calculations, a 1 nm dipole is positioned at various locations in the plane 15 nm inside the aperture. The radiative emission is estimated from the quartz side by integrating the z component of Poynting vectors across a plane located 20 nm below the metal surface. This power is then compared to the emission in the absence of the nanoaperture. Calculations are performed for x, y, and z dipole orientations, and the reported radiative enhancement is an average for these orientations. Figure 6 displays the emission enhancement factors versus the aperture diameters for gold and aluminum films (filled markers). A clear effect is seen between gold and aluminum, with 2.5 times more favorable emission enhancement in the case of gold. This is fully consistent with the higher count rates observed for gold at fluorescence saturation (a factor of 2.8 experimental). This factor is also in agreement with the two times larger saturation intensity found for gold in Fig. 3 (the saturation intensity is proportional to the ratio of the total decay rate to the excitation cross section, hereby indicating a larger increase of decay rate than excitation power when comparing gold to aluminum). At low excitation powers (below fluorescence saturation), the gain due to emission in the overall detected signal is lower, as it depends on the fluorophore quantum yield which interplays radiative and nonradiative rates. Starting from the gain in emission rate presented in Fig. 6 and given the quantum yield of A647 in solution of 30%, we infer a maximum quantum yield of 70% for A647 in a 120 nm gold aperture, and 50% for A647 in a 170 nm aluminum aperture. Therefore, the relative difference between the quantum yield gains for gold and aluminum is estimated to be about 40%. Again, this factor directly contributes to the better fluorescence enhancement obtained for gold apertures.

To predict the optimal diameter for aperture-enhanced fluorescence, we computed the propagation constant γ of the fundamental guided mode inside an infinitely long cylindrical aperture as a function of the aperture diameter (Fig. 7). The inner medium was taken to be water (refractive index of 1.33). The computation is based on the differential method written in a cylindrical geometry.[41] γ is defined as $\gamma = k_z / k_0$, where $k_0 = 2\pi/\lambda$. For apertures through a perfectly conducting metal, the cutoff is defined as the size of the aperture where the real part of the propagation constant γ vanishes. If the aperture is smaller than the cutoff, γ becomes imaginary and no propagative guided mode exists. Moreover, at the cutoff, the group velocity v_g equals zero. In the presence of absorption, γ becomes complex valued and, strictly speaking, there is no cutoff as the propagation constant never equals zero. A cutoff can still be defined, though. Following the intuitive definition of Baida *et al.*,[11] we define the cutoff as the size where the imaginary part of γ becomes higher than its real part: this corresponds to the crossing point of the curves plotted in Fig. 7. The corresponding position is shown in Fig. 7 as vertical dashed lines. Also indicated with arrows in Fig. 7 is the position of the maximum fluorescence emission enhancement $\eta_{\max}$ (taken from Fig. 2). Surprisingly, the optimum diameter for fluorescence enhancement falls about 50 nm below the intuitive cutoff diameter. To clarify this discrepancy, it should be stressed that for absorbing materials, the crossing between the real and imaginary parts of γ does not correspond anymore to a zero group velocity. For a real metal, v_g never vanishes, but passes through a minimum when the real part of γ is minimum. This corresponds to a maximum of the photonic density of modes.[43] This point is shown in Fig. 7 as a black dot. It appears that the observed position of $\eta_{\max}$ is very close to the position of the minimum group velocity. Therefore, we relate the maximum field enhancement inside the aperture to a maximum density of photonic modes and to a minimum group velocity. The significant shift of the optimum diameter as compared to the intuitive position of the cutoff has to be considered while designing nanoapertures for optimized single-molecule analysis.

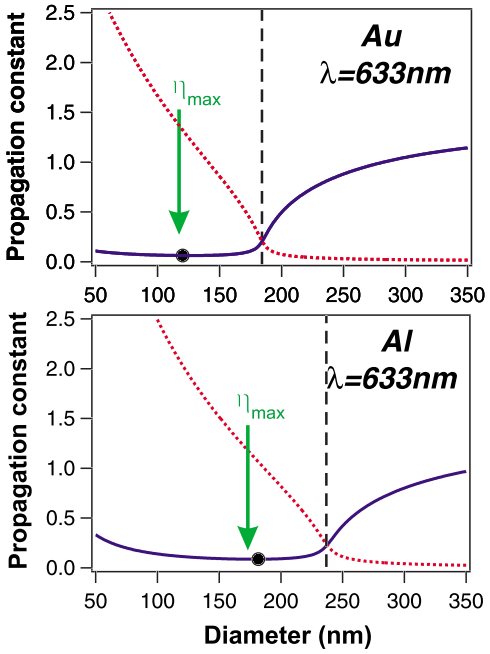

FIG. 7. (Color online) Propagation constant γ of the fundamental guided mode inside the aperture vs aperture diameter for gold and aluminum films, the aperture being filled with water. Solid line, real part of γ; dotted line, imaginary part of γ. The vertical dashed lines show the intuitive position of the cutoff, the arrows indicate the position of the observed maximum enhancement factor $\eta_{\max}$, and the dots show the position of the minimum group velocity [minimum value of Re(γ)].

As a final test experiment, we have performed measurements for gold apertures at $\lambda_e = 488$ nm excitation wavelength, using Rhodamine6G as a fluorescent molecule (Fig. 8). In this case, a rather low enhancement factor is found ($\eta \sim 2.5$) that only weakly depends on the aperture size. To understand these results, one has to recall that at this excitation wavelength, gold behaves more like a highly absorbing dielectric than like a metal. On the other hand, detection was performed in the range of 550–590 nm, where gold has a strong metallic behavior. Using the same experimental conditions, apertures milled in aluminum were shown to yield larger enhancement factors.[28] The inset of Fig. 8 presents the calculated propagation constants for the corresponding apertures: there is no cutoff as the real part of γ never approaches zero. Therefore, the group velocity never reaches low values.

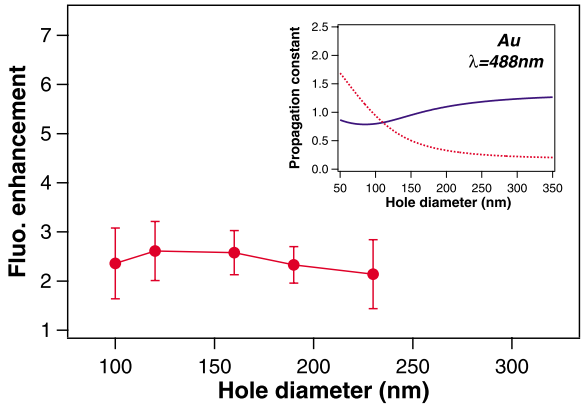

FIG. 8. (Color online) Enhancement factor as a function of the aperture diameter for Rhodamine 6G dyes excited at λ_e=488 nm for nanoapertures milled in a gold film. Inset: Calculated propagation constant γ of the fundamental guided mode inside the gold aperture (solid, real part; dots, imaginary part).

This demonstrates the crucial importance of milling the nanoaperture in a material that exhibits a strong metallic character at the excitation wavelength. The strong electromagnetic field confinement induced by the metallic nanocavity is confirmed to be a key factor in the aperture-enhanced fluorescence process.

V. CONCLUSION

Using fluorescence correlation spectroscopy, we have rigorously characterized the fluorescence emission enhancement factors η for dyes freely diffusing in nanometric apertures milled in gold and aluminum films. We have observed that apertures milled in gold exhibit significantly higher fluorescence enhancement factors than apertures milled in aluminum. We demonstrate that the higher value of η for gold is related to a larger enhancement of the excitation intensity and radiative rate. The maximum enhancement for gold also occurs at a smaller aperture diameter, which is beneficial for single-molecule detection at high concentrations. Moreover, the enhancement covers the entire emission spectrum of the dye and shows only slight spectral variations. We have shown that the maximum value of η is obtained when the group velocity of the guided mode inside the aperture is close to zero, that is, when the photonic density of modes is maximum. This diameter is significantly shifted (up to 50 nm) as compared to the intuitive position of the cutoff of the fundamental guided mode. This effect has to be taken into account while designing nanoapertures for high-efficiency single-molecule analysis. Let us finally emphasize that nanoapertures, in spite of their conceptual simplicity, demonstrate unique and appealing properties for controlling fluorescence emission. These properties are of great interest to increase the effectiveness of fluorescence-based techniques.

ACKNOWLEDGMENTS

This work has been funded by Grant No. ANR-05-PNANO-035-01 "COEXUS" of the French National Research Agency. F.M. and S.B. were supported in part by National Science Foundation Grants No. ECS-0622225 and No. ECS-0637121.

[1] H. G. Bethe, Phys. Rev. **66**, 163 (1944).
[2] T. W. Ebbesen, H. J. Lezec, H. F. Ghaemi, T. Thio, and P. A. Wolff, Nature (London) **391**, 667 (1998).
[3] J. A. Porto, F. J. Garcia-Vidal, and J. B. Pendry, Phys. Rev. Lett. **83**, 2845 (1999).
[4] H. J. Lezec, A. Degiron, E. Devaux, R. A. Linke, L. Martin-Moreno, F. J. Garcia-Vidal, and T. W. Ebbesen, Science **297**, 820 (1998).
[5] E. Popov, M. Nevière, J. Wenger, P.-F. Lenne, H. Rigneault, P. Chaumet, N. Bonod, J. Dintinger, and T. W. Ebbesen, J. Opt. Soc. Am. A **23**, 2342 (2006).
[6] A. Naber, D. Molenda, U. C. Fischer, H.-J. Maas, C. Höppener, N. Lu, and H. Fuchs, Phys. Rev. Lett. **89**, 210801 (2002).
[7] C. Genet and T. W. Ebbesen, Nature (London) **445**, 39 (2007).
[8] H. Shin, P. B. Catrysse, and S. Fan, Phys. Rev. B **72**, 085436 (2005).
[9] M. Bai and N. Garcia, Appl. Phys. Lett. **89**, 141110 (2006).
[10] F. J. García-Vidal, L. Martin-Moreno, E. Moreno, L. K. S. Kumar, and R. Gordon, Phys. Rev. B **74**, 153411 (2006).
[11] F. I. Baida, A. Belkhir, D. Van Labeke, and O. Lamrous, Phys. Rev. B **74**, 205419 (2006).
[12] S. Collin, F. Pardo, and J.-L. Pelouard, Opt. Express **15**, 4310 (2007).
[13] J. R. Lakowicz, Anal. Biochem. **337**, 171 (2005).
[14] P. Anger, P. Bharadwaj, and L. Novotny, Phys. Rev. Lett. **96**, 113002 (2006).
[15] S. Kühn, U. Håkanson, L. Rogobete, and V. Sandoghdar, Phys. Rev. Lett. **97**, 017402 (2006).
[16] F. Tam, G. P. Goodrich, B. R. Johnson, and N. J. Halas, Nano Lett. **7**, 496 (2007).
[17] Y. Chen, K. Munechika, and D. S. Ginger, Nano Lett. **7**, 690 (2007).
[18] J. S. Biteen, L. A. Sweatlock, H. Mertens, N. S. Lewis, A. Polman, and H. A. Atwater, J. Phys. Chem. C **111**, 13372 (2007).
[19] P. Bharadwaj and L. Novotny, Opt. Express **15**, 14266 (2007).
[20] J. S. Biteen, D. Pacifici, N. S. Lewis, and H. A. Atwater, Nano Lett. **5**, 1768 (2005).
[21] G. L. Liu, J. Kim, and L. P. Lee, Appl. Phys. Lett. **89**, 241118 (2006).
[22] Y. Liu and S. Blair, Opt. Lett. **28**, 507 (2003).
[23] A. G. Brolo, S. C. Kwok, M. D. Cooper, M. G. Moffitt, C.-W. Wang, R. Gordon, J. Riordon, and K. L. Kavanagh, J. Phys. Chem. B **110**, 8307 (2006).
[24] Y.-J. Hung, I. I. Smolyaninov, C. C. Davis, and H.-C. Wu, Opt. Express **14**, 10825 (2006).
[25] G. Sun, J. B. Khurgin, and R. A. Soref, Appl. Phys. Lett. **90**,

111107 (2007).
[26] J. H. Kim and P. J. Moyer, Appl. Phys. Lett. **90**, 131111 (2007).
[27] U. C. Fischer, J. Opt. Soc. Am. B **3**, 1239 (1986).
[28] H. Rigneault, J. Capoulade, J. Dintinger, J. Wenger, N. Bonod, E. Popov, T. W. Ebbesen, and P.-F. Lenne, Phys. Rev. Lett. **95**, 117401 (2005).
[29] J. Wenger, B. Cluzel, J. Dintinger, N. Bonod, A.-L. Fehrembach, E. Popov, P.-F. Lenne, T. W. Ebbesen, and H. Rigneault, J. Phys. Chem. C **111**, 11469 (2007).
[30] M. J. Levene, J. Korlach, S. W. Turner, M. Foquet, H. G. Craighead, and W. W. Webb, Science **299**, 682 (2003).
[31] K. T. Samiee, M. Foquet, L. Guo, E. C. Cox, and H. G. Craighead, Biophys. J. **88**, 2145 (2005).
[32] H. G. Craighead, Nature (London) **442**, 387 (2006).
[33] J. T. Mannion and H. G. Craighead, Biopolymers **85**, 131 (2006).
[34] W. L. Barnes, J. Mod. Opt. **45**, 661 (1998).
[35] *Fluorescence Correlation Spectroscopy: Theory and Applications*, edited by R. Rigler and E. L. Elson (Springer-Verlag, Berlin, 2001).
[36] C. Obermüller and K. Karrai, Appl. Phys. Lett. **67**, 3408 (1995).
[37] A. Degiron, H. J. Lezec, N. Yamamoto, and T. W. Ebbesen, Opt. Commun. **239**, 61 (2004).
[38] L. Dai, I. Gregor, I. von der Hocht, T. Ruckstuhl, and J. Enderlein, Opt. Express **13**, 9409 (2005).
[39] F. Bordas, N. Louvion, S. Callard, P. C. Chaumet, and A. Rahmani, Phys. Rev. E **73**, 056601 (2006).
[40] E. Popov, M. Nevière, A. Sentenac, N. Bonod, A.-L. Fehrembach, J. Wenger, P.-F. Lenne, and H. Rigneault, J. Opt. Soc. Am. A **24**, 339 (2007).
[41] N. Bonod, E. Popov, and M. Nevière, J. Opt. Soc. Am. A **22**, 481 (2005).
[42] F. Mahdavi, Y. Liu, and S. Blair, Plasmonics **2**, 129 (2007).
[43] *Nanophotonics*, edited by H. Rigneault, J.-M. Lourtioz, C. Delalande, and A. J. Levenson (ISTE, London, 2006).